DOI: 10.13009/EUCASS2022-7234

Sizing Superconducting motor associated with cryogenics power electronics for disruptive hybrid electric propulsion aircrafts

*Jean Lévêque****, Rémi Dorget*,****, Min Zhang***, Abdelrahman Elwakee***l, Christophe Viguier**, Sabrina Ayat**

** SAFRAN TECH, Magny-les-Hameaux*

*** SAFRAN TECH, Blagnac*

**** UNIVERSITY OF STRATHCLYDE (USTRATH) Glasgow*

***** GREEN Université de Lorraine*

Abstract

This paper presents some results of the investigations carries out in the frame of the IMOTHEP project (Investigation and Maturation of Technologies for Hybrid Electric Propulsion). This European project aims to study the potential of hybrid and electric propulsion on different aircraft concepts, from Regional to Short Medium Range aircrafts, to reduce the fuel consumption and CO2 emissions. For each concept, two approaches are defined: a conservative (close to conventional aircraft) and a radical (to consider disruptive options). The focus is done on the disruptive aircraft configuration.

1. Introduction

In this paper, a basic review of switches performance has been done to estimate the most suitable device. IGBT's were found most suitable due to their good performance at cryogenic temperature and their availability at the required rating for the inverter. Then a quick comparison has been done between different inverter topologies, where it was shown that the NPC has the best performance as it is the most efficient and most suitable for the motor application. Then, a comparison between NPC and ANPC has shown that by replacing the diodes with IGBT's, better performance can be obtained. Then, in the end, a technique for calculation of the converter losses and initial weight estimation has been done. It is possible with a fully superconducting machine to achieve a very high-power density. The role of the input is not decisive, and it can therefore be easily adapted to the technical choices that will be made. Torque oscillations are low, less than 10% for all configurations. The main remaining problem is that of optimization, considering the losses in the superconductors and the non-active elements of the machine.

1. Context: the decarbonization of civil aviation

1.1 Climate impact of the aeronautical sector

The year 2019 marks a record for global greenhouse gas emissions with an annual total of 52.4 Gt CO2eq [1]. Although the COVID-19 health crisis led to a drop-in emission in 2020, 2021 emissions have almost caught up to their pre-crisis level [2]. Within the total CO2 emissions due to energy consumption, the transport sector is particularly emitting with a share of about 25% [3]. Aviation is the second mode of transport in terms of global emissions, far behind road transport but equivalent to maritime transport, representing 11% of total transport, or 920 Mt CO2 in 2019 [4]. At first glance, the climate impact of aviation seems relatively limited compared to other polluting sectors. Despite the limited global impact of aviation, the impact of air transport on an individual's carbon footprint is very significant, since a round trip from Paris to New York emits 1 t of CO2, whereas the average annual carbon footprint of a French person is 8 t CO2eq. The main technological lever for reducing CO2 emissions is to continue the effort to improve the energy efficiency of aircraft.

An important movement is the replacement of pneumatic and hydraulic actuators by electric actuators in order to increase the reliability and reduce the size of a number of components performing non-propulsive functions of the aircraft [5]-[7]. The following examples can be cited in particular:

This project has received funding from the European Union's Horizon 2020 research and innovation program under grant agreement No 875006 IMOTHEP

DOI: 10.13009/EUCASS2022-7234

Engine starting is traditionally provided by pneumatic actuation, but this function has recently been electrified on the Boeing 787.

- The electrification of flight controls by replacing hydraulic actuators with electro-hydrostatic actuators for the most critical functions and electro-mechanical actuators for the less critical ones.
- The air conditioning is traditionally ensured by taking air from the engines inducing a loss of performance of the latter. To compensate for this, the latest Boeing 787 replaces this air sampling with four 100 kW electric compressors.
- In a similar way, the de-icing and anti-icing is also generally ensured by taking hot compressed air on the engines. This function can also be electrified by installing heating mats on the parts of the wing to be protected. This alternative is more energy efficient but requires 150 kW of electrical power on the Beoing 787 for example.
- Thus, the electrification of all these functions results in an increase in the electrical power installed on board the aircraft. The 787 being the most electric commercial aircraft, it has 4 250 kVA generators connected to the engines and 2 225 kVA generators on the APU (Auxiliary Power Unit) [7].

1.2 Electric and hybrid propulsion

Like the automotiv the electrification of aircraft propulsion functions is also an important potential lever for reducing the climate impact of aviation. However, the storage of electrical energy on board an aircraft is more complex than on board a car. There is a large number of possible architectures integrating total or partial electric propulsion [8], [9].
The main disadvantage of batteries is their mass energy density, which is considerably lower than that of kerosene or LH2. For lithium-ion batteries, this is of the order of 0.2 kWh/kg. Thus, fully electrified architectures with batteries seem to be limited only to light aircraft not exceeding a few tons of take-off weight [10]. However, for the regional aircraft segment, a parallel hybridization with batteries may be of interest. For example, theoretical studies have estimated that a 30% hybridization rate could lead to an 8% reduction in fuel consumption for a 2400 km mission or even a 28% reduction for a 1500 km mission [11]. However, these studies were performed assuming batteries with a specific energy density of 1 to 1.5 kWh/kg implying a significant improvement compared to the current state of the art [12].
The partially turboelectric architecture consists in transforming part of the mechanical energy of the aircraft's turbofan engines into electrical energy in order to power one or more electric motors driving propellers placed at specific locations of the aircraft in order to obtain an aerodynamic gain. However, the viability of these architectures is strongly dependent on the performance of the components of the electrical chain. Indeed, the electrical chain placed between the turbomachines and the propellers increases the weight of the aircraft and generates losses that have an impact on fuel consumption. Thus, for an architecture to be interesting, it is necessary that the reduction in consumption brought by the aerodynamic gains exceeds the additional consumption due to the mass of the electrical chain and its losses. A NASA study [13] tried to estimate the profitability threshold of a completely turboelectric architecture according to the efficiency of the electrical chain. This study concludes that an overall specific power of the electrical chain of 15 kW/kg is required for an efficiency of 94% while 10 kW/kg is sufficient for an efficiency of 98%.
All the electrical architectures we have just reviewed have in common that they require electrical components (motors, cables and static converters) with high power-to-weight ratio and high efficiency in order to reduce the energy requirement of the aircraft to a minimum. In this section, we will discuss the performance of these components and especially of the electrical machines

1.2.1 Conventional electrical power train

The current state of the art of the components of an electric chain make it difficult to reach the objectives of efficiency and power density that we have previously cited for a completely turboelectric configuration [13]. Indeed, according to a state of the art of 2019, the machines whose speed is lower or equal to 4000 rpm, reach a power density of 5 kW/kg for an efficiency of 95% [14], [15]. Machines with speeds closer to 20,000 rpm, can achieve 8 kW/kg and 97% efficiency [14]. Thus, these values alone fall short of the goal of the NASA study. However, several levers are available to seek to reduce the mass of electric motors:

- Reduce the mass of non-active mechanical parts by optimizing the mechanical structures [14].
- Cooling the armature of electric machines to increase current densities [16]-[18].
- Increase the frequency and polarity of the machines to reduce the size of the magnetic yokes.

By incorporating some of these solutions, a 4 MW, 17,000 rpm generator was realized in 2021 reaching 17 kW/kg and 97% efficiency [18].

This project has received funding from the European Union's Horizon 2020 research and innovation program under grant agreement No 875006 IMOTHEP

DOI: 10.13009/EUCASS2022-7234

1.2.2 Cryogenic electrical power train

The current state of the art of the classical components of an electrical chain makes it difficult to reach the objectives of efficiency and power density for a completely turboelectric configuration [13]. A technological breakthrough could be the use of a cryogenic and superconducting electrical chain in order to have much more efficient components. This solution includes superconducting electrical machines and cables requiring operation at temperatures below 77 K as well as static converters, non-superconducting, but whose operation is improved at very low temperatures. This solution has been considered by NASA to allow turboelectric propulsion, [19]. Indeed, superconductors allow to reach very high current and magnetic flux densities which can allow a drastic reduction of the size of electrical machines. In addition, the losses in superconductors are zero in direct current and potentially much lower than resistive materials in alternating current, allowing a very significant improvement in efficiency. In addition to a potential gain in mass and efficiency, the use of superconducting cables could allow the distribution of electrical energy at low voltage.
A distinction is generally made between machines with a superconducting inductor and those with a superconducting armature. The superconducting inductor has been particularly studied in the context of superconducting machines for wind and naval applications [23]-[26] and can be adapted to aeronautical applications. Thus, a theoretical design of a 10 MW, 7000 rpm superconducting rotor generator could achieve 23 kW/kg and 98% efficiency [24]. Machines with a superconducting armature, on the other hand, have a much higher potential performance, whether or not they are associated with a superconducting inductor. The reduced losses in the superconducting armatures make it possible to envisage efficiencies of the order of 99.9% for power densities greater than 30 kW/kg [20]-[22]. It should be noted, however, that 0.1% of losses on a high-power machine is still a very large amount of losses for a cryogenic system. The extraction of these losses could be done, as envisaged in the NASA studies, by the use of cryocoolers, [19]. However, at 20 K, commercial cryocoolers correspond to a thermal management coefficient of 3300 kg/kW of losses [28], [29], ambitious projects of cryocoolers adapted to on-board applications have been initiated by NASA in order to reduce their weight to 550 kg/kW at 20 K [29]-[31] but these values remain high. The recent development of studies and projects for the use of LH2 as fuel could represent a very interesting alternative to cryocoolers. Indeed, the need to warm up LH2 before its use presents a synergy with the cooling of the components of a cryogenic power train. Thus, the use of superconducting armature machines seems quite feasible in an LH2 aircraft but difficult in a configuration with cryocoolers.
Concerning superconducting cables, this is a very mature technology for ground applications in the electrical network [32], and its adaptation to an onboard use seems to be simpler. However, the few existing public works explore several cable architectures and the associated soldering problems [33]. Studies on cryogenic power electronics are much less advanced and are usually limited to component tests [34]-[38] but the structural changes to be implemented are less important insofar as the materials are identical, only used in a different environment. We can however mention the realization of a 1 MW inverter at the University of Tennessee with the support of NASA and Boeing [39]-[41].

2. Superconductors properties

Superconducting wires and by extension coils made with them can only operate under certain temperature and induction conditions. Therefore, it is important to understand and model correctly the behavior of the wires inside and at the limit of their operating range
The critical current Ic of each superconducting wire depends on the magnetic field, its application angle, and the temperature according to a different I_c (B,θ,T) characteristic for each wire. Therefore, each wire must be properly characterized before it can be used. For HTS Bi-2223 (1G) and REBaCuO (2G) tapes, the University of Wellington maintains a database by characterizing tapes from different manufacturers [123], [124]. From this database, Figure 1 shows the critical current of tapes from several manufacturers at 77 K and 20 K as a function of the magnetic field when applied at the most critical angle. It can be seen that the performance and the shape of the characteristics are very different from one tape to another. At 20 K, for example, the SuperOx tape has a higher critical current at low field than the Fujikura tape but the latter resists better at high magnetic field, the curves crossing around 1 T. Moreover, some wires have excellent performances at 77 K but much less at 20 K like the THEVA tape for example.

This project has received funding from the European Union's Horizon 2020 research and innovation program under grant agreement No 875006 IMOTHEP

DOI: 10.13009/EUCASS2022-7234

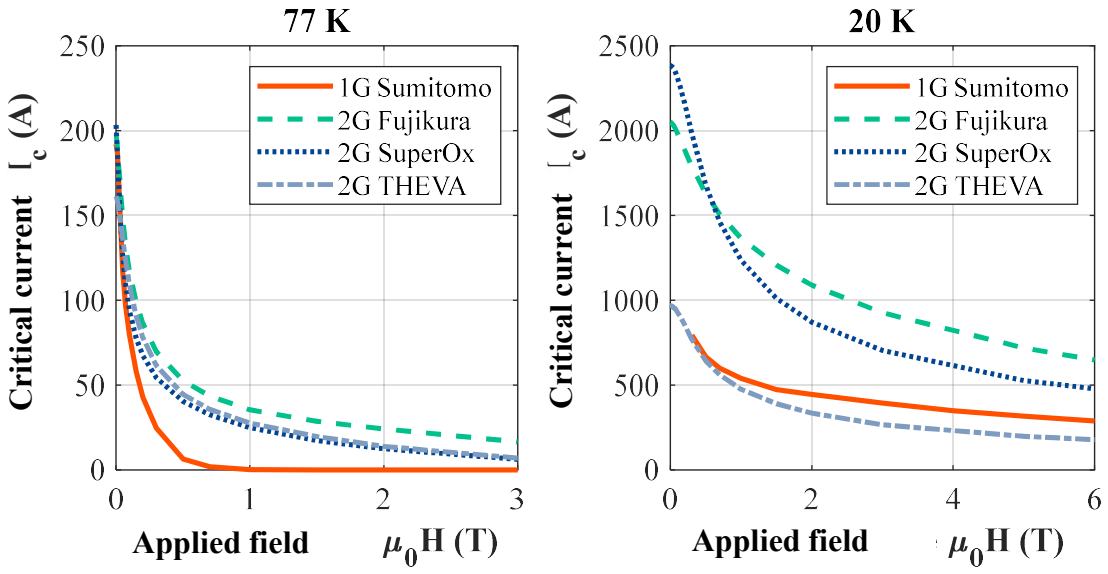

Figure 1 Critical current of several 4 mm wide HTS ribbons at 77 K (left) and 20 K (right) as a function of the magnetic field when applied at its most critical angle [42], [43]

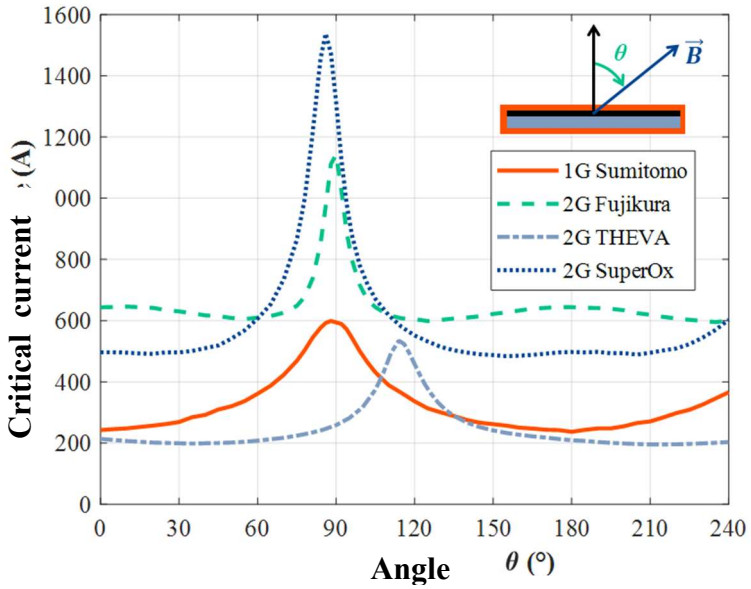

Figure 2 Dependence of the critical current on the angle of the applied magnetic field of different HTS tapes for a temperature of 30 K and a field of 3 T. An angle of 0° corresponds to a magnetic field perpendicular to the tape

Moreover, the magnetic field dependence also strongly depends on the angle of application of the magnetic field θ as shown in Figure 2. Indeed, we see that for a Bi-2223 wire at 30 K and a field strength of 3 T for example, the critical current is almost 3 times higher when the field is parallel to the wire (θ=90°) than when the field is perpendicular (θ=0°). As a general rule, the most favorable case is found to be when the magnetic field is parallel and the most defavorable case when the magnetic field is perpendicular, as for Bi-2223. However, we note that some wires deviate particularly from this tendency, such as THEVA tape for example, whose deposition method involves a different crystalline orientation giving a maximum at 114°. Similarly, the Fujikura ribbon at 30 K is at its minimum critical current between 0° and 70° depending on the amplitude of the field while its maximum is always around 90°

This project has received funding from the European Union's Horizon 2020 research and innovation program under grant agreement No 875006 IMOTHEP - Copyright© 2022 by IMOTHEP. Published by the EUCASS association with permission.

DOI: 10.13009/EUCASS2022-7234

2. Superconducting motor design

The power density in a motor is proportional to the fields created by the armature and the inductor, as can be seen in the following relationships:

$$P = \frac{\pi}{2}\ m\ \frac{f}{p} \qquad K_p\ K_i\ K_s\ B_r\ A_s\ \ LD^2 \tag{1}$$

- m: number of phases,
- p: number of poles,
- Kp, Ki, Ks: coefficients depending on the shape of the current and the winding,
- Br is the magnetic field created by the inductor
- As is the magnetic field create by armature

$$PtM = \frac{\pi}{2}\ m\ \frac{f}{p} \qquad K_p\ K_i\ K_s \quad B_r\ A_s \tag{2}$$

we have the coefficients we can play with. There are therefore only two possibilities to increase the power density:
Increase the field created by the inductor,
Increase the field created by the armature.

The main limitations are as follows: the induction is limited by the saturation of the ferromagnetic elements. In addition, the use of permanent magnets limits the induction in the air gap of the machine due to their limited remanent field. So, the majority of industrial applications are radial flux synchronous motors. The most natural choice is therefore to have stator and rotor windings.
In the stator, the windings will be placed in the air, without ferromagnetic teeth with a simple flux return yoke. These stator windings are subject to alternating magnetic fields which generate additional losses: eddy current losses and circulating current losses. The latter can be reduced by an appropriate choice of conductor size (Litz wire) and twisting. One solution is also to consider superconducting windings. The increase in current density allows the volume of the conductors to be reduced and consequently the electric load to be increased. On the other hand, the cold losses in superconducting materials can become prohibitive. This determines the type of material used. We have a choice of first generation BSCCO wires, second generation Re-BCO wires, and MgB2 wires for high temperature materials. The current density as a function of the magnetic field is highest for ReBCO-based wires, but MgB2 wires are easier to twist and it is easier to make them multi-filament, thus reducing losses. In addition, they are significantly cheaper.
Different rotor designs use or do not use iron to create a magnetic circuit in the cold end. Rotors without a ferromagnetic core are called ironless rotors. In this case, a non-magnetic structuring material is used instead of iron, usually based on a glass fiber composite, which is used as a support for the superconducting coils. There are two possible ways of designing rotors with a ferromagnetic core: either the core is placed at cryogenic temperature (cold iron-cored rotor) or at room temperature (warm iron-cored rotor). This point has a direct impact on the volume of the machine
In the case of a fully superconducting machine, we also have several possible choices, either the cryogenic enclosure encompasses the stator and rotor windings, or there are two separate cryostats. The influence is great since it conditions the value of the air gap.
The specification of the prototype we are designing is summarized:

- Speed 3380 rpm
- Power 2,3 MW

2.1 Working assumptions

The operating temperature is one of the key points of the project. We arbitrarily choose to work at the temperature of liquid hydrogen, 20K. At this temperature, the properties of the ReBCO tapes are excellent and those of the MgB2 correct.
We make two assumptions:

- the first is that of two separate cryostats, one for the stator and the other for the rotor, which imposes an air gap of at least 20 mm;
- the second working assumption is that of a common cryostat which allows the air gap to be reduced to 5 mm.

For this project, we have chosen a radial synchronous machine with a wound rotor. It is a very classical synchronous motor but, with a full superconducting coil, we expect good performances.

This project has received funding from the European Union's Horizon 2020 research and innovation program under grant agreement No 875006 IMOTHEP

DOI: 10.13009/EUCASS2022-7234

2.2 Design

We made two studies, the first one with a small airgap and the second one with a low airgap. By air gap, we mean the distance between the coils of the inductor and the armature. These studies need to be completed as a first step to determine the total losses of the machine that will influence the final dimensions.
As this is only a first design, we have not evaluated the overall losses of the machine including the thermal losses. The consumption of cryogenic fluid will be the subject to further study when the geometrical dimensions of the machine will be finalized
In this study, we have reduced the air gap considerably. This has just reduced the size of the machine without affecting the power density. The solutions with one or two cryostats are therefore equivalent.

Table 1: Synthesis of the main data for the first design for small airgap

Parameter	Value	Unit
Length	200	mm
Radius of the machine	140	mm
Thickness of backiron	20	mm
Stator slot depth	10	mm
Number of stator slot	6	
Airgap	5	mm
Rotor slot depth	10	mm
Number of rotor slot	8	
Thickness of rotor backiron	10	mm
Current density in stator	100	A/mm^2
Bmax on stator coil	1.8	T
Current density in rotor	500	A/mm^2
Bmax on Rotor coil	1.08	T
Power	2.6	MW
Power to Mass ratio	51	kW/kg

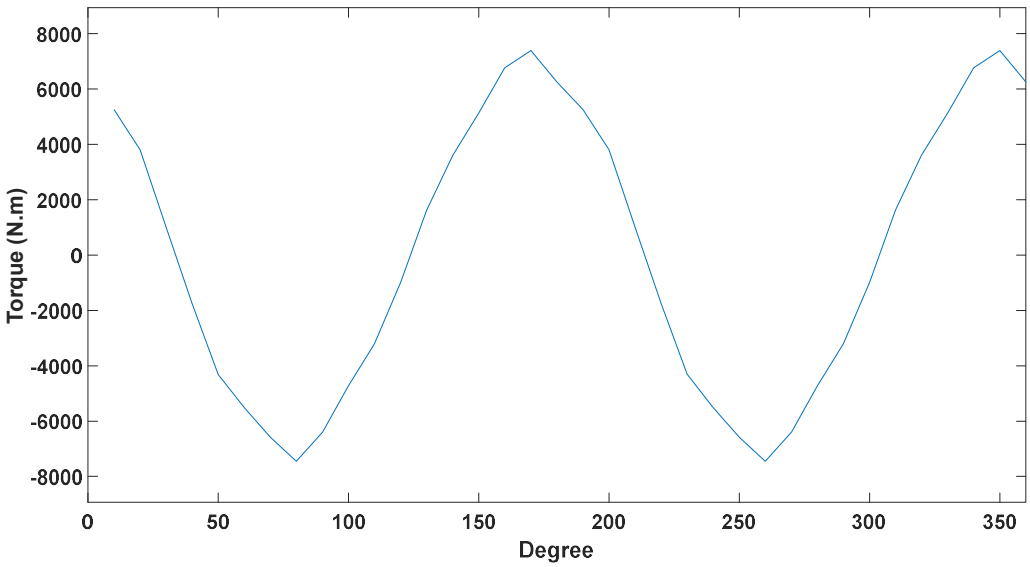

Figure 3: variation of the torque with angle

This project has received funding from the European Union's Horizon 2020 research and innovation program under grant agreement No 875006 IMOTHEP - Copyright© 2022 by IMOTHEP. Published by the EUCASS association with permission.

DOI: 10.13009/EUCASS2022-7234

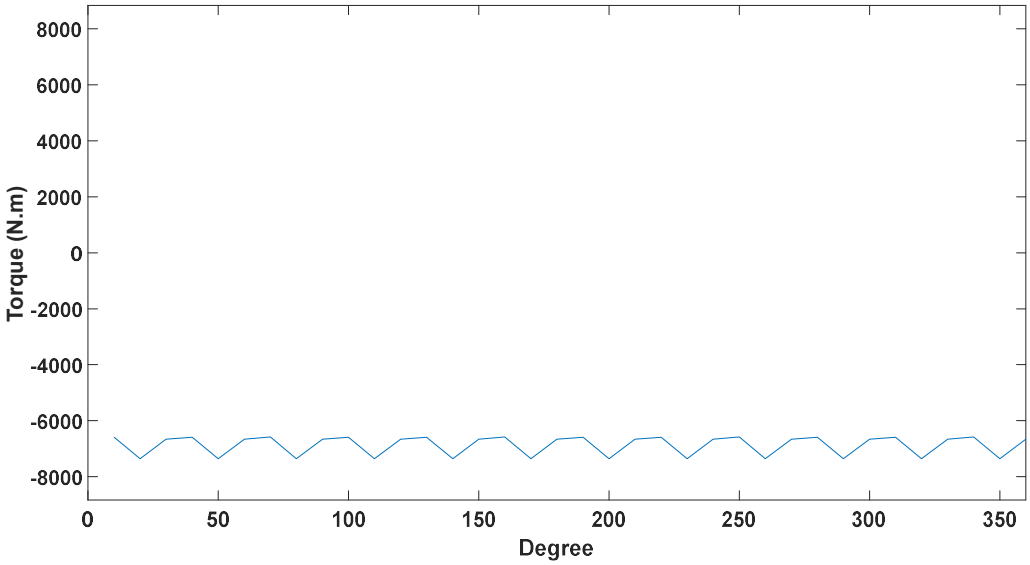

Figure 1: Ripple torque for a high airgap

2.3 Cooling design

One of the key points of a superconducting motor or generator is to keep the system cold. This has to be linked with a very strong constraint, in the case of aeronautical applications, which is the weight of the total system. The main problem with cold generation systems is their mass and their high footprint, which can be greater than that of the motor. It is also possible to dispense with any onboard refrigeration system and operate with an enthalpy reserve for the duration of the flight mission. The superconducting motor will be cooled down when the aircraft is stopped at the airport.
The main loss items in a superconducting motor are as follows:

- Losses in the superconductors, these losses are small and perfectly negligible in direct current, we will not take them into account. On the other hand, these losses are very important and can become prohibitive for the armature's AC powered windings.
- The losses of the cryostat are multiple. There are radiation losses that are easily reduced by the use of anti-radiation heat shields such as super-insulation. The connection losses between the cold coils and the hot wall of the cryostat can be important and we will study them. The losses by gaseous convection are perfectly negligible when a high vacuum is applied.
- The last loss item is the current supply to the superconducting coils, which will be calculated.

2.3.1 Radiation losses

These are losses without material support by pure electromagnetic radiation. These losses between two walls at different temperatures can be calculated using Stephan's law:

$$W_{radiation} = \sigma \, F_{12} \, S_1 (T_2^4 - T_1^4) \qquad (3)$$

This is true with the assumption of a grey body, i.e. the emissivity of materials is assumed to be independent of wavelength. Sigma is Stephan's constant of 5.67 10^{-8} W/m^{2}K^4.
F_{12} is a form factor depending on the emissivities, we recall it in some classical cases.
Between two flat surfaces facing each other, with identical surface area:

$$F_{12} = \frac{\varepsilon_1 \varepsilon_2}{\varepsilon_2 + (1-\varepsilon_2)\varepsilon_1} \qquad (4)$$

Between two coaxial cylinders, of large length compared to the radius, one designates the inner tube and two the outer tube:

This project has received funding from the European Union's Horizon 2020 research and innovation program under grant agreement No 875006 IMOTHEP

DOI: 10.13009/EUCASS2022-7234

$$F_{12} = \frac{\varepsilon_1 \varepsilon_2}{\varepsilon_2 + \frac{S_1}{S_2}(1-\varepsilon_2)\varepsilon_1} \quad (5)$$

In general, cryogenics experts use the following relationship for close surfaces with low emissivity:

$$W_{rayonnement} = 0{,}5\ \sigma\ \ \varepsilon\ S_1\ (T_2^4 - T_1^4) \quad (6)$$

It is important to have surfaces with the lowest possible emissivity to reduce these losses. As an example, we present results valid between 300 K and 30 K, for two flat plates facing each other with the same emissivity. For an emissivity of 0.1, we obtain 25W/m^2 of losses, and for an emissivity of 0.01, we obtain 2.3 W of losses. This indicates the importance of reducing emissivity.
The losses are usually reduced considerably by inserting a screen at 80 K cooled by nitrogen which absorbs the essential part of the losses. In our case, we want to be free of any onboard refrigeration machine, so there is no question of having a screen cooled by a cryocooler at 77 K. We will therefore choose another solution, which is that of passive screens. These passive screens are aluminum sheets insulated with mylar to avoid thermal conduction. These sheets are wrapped around the surfaces to be protected with several layers adjusted both by the space available and the level of losses as shown in the following figure. As electromagnetic radiation is involved, the surface to be protected must be optically invisible. With super-insulation, the reduction of radiation losses is given by the following simple relation:

$$W_{super\ isolant} \approx W_{rayonnement} \frac{1}{nombre\ de\ couche+1} \quad (7)$$

We can take examples with a temperature variation between 300K and 30K

The losses between 300 K and 30 K with an emissivity of 0.1 are 24.15 W/m^2
The losses between 300 K and 30 K with an emissivity of 0.01 are 2.3 W/m^2
The losses between 300 K and 30 K with an emissivity of 0.1 and 10 layers of super insulation are 2.2 W/m^2

2.3.2 Solid conduction losses

These are the losses in the elements that hold the solenoids in the cryostat. To evaluate the losses, we use a numerical simulation and an analytical calculation. To simulate numerically we bring all the radiation losses back to the fiberglass parts that support the coils and also make the link between the hot and cold parts. Then, we consider the heat exchanger designed to cool the superconducting coils. This heat exchanger is assumed to be at a constant temperature.
This does not consider the cooling mode, we simply have the contacts with the cryostat wall imposed at 300 K, the contacts with the exchanger imposed at 20 K, and the elements for which a heat flux corresponding to the radiation losses is imposed. The materials used are G11 and superconductor
The losses are estimated at 30 W.

2.3.3 Losses in the current leads

The losses in the current conductors are the contribution of the joule losses and the thermal losses by conduction. We can express the joule and thermal losses as a function of the ratio of length to the cross-section of the current leads. Typically, these losses are at least 50W/kA/m, in our case, it is 50 W

2.3.4 Losses in the Armature

These losses are very important and particularly complex to calculate. This is still the subject of much research. These losses depend mainly on the materials used, the magnetic field to which they are subjected, and the frequency of the supply currents.
The table 2 given is an initial assessment of these losses and will have to be the subject of a much more complete future development. The first estimate is 7 kW.

This project has received funding from the European Union's Horizon 2020 research and innovation program under grant agreement No 875006 IMOTHEP

DOI: 10.13009/EUCASS2022-7234

Figure 2: Losses

Losses	Value
Conduction losses	≈ 30 W
Radiative losses	≈ 3 W
Current lead	≈ 50 W
DC current losses	Neglectable
AC Losses (from review)	**≈ 7 kW**

2.3.5 Cryogenic fluid consumption

Hydrogen is the most favorable gas in terms of mass and volume. Hydrogen, even as a liquid, has a very high specific heat and it is not necessary to solidify it, so it can be used between 10 and 20 K, even recovering the very high latent heat of change of state. A quick estimate of the amount of cryogenic fluid results in a consumption of 55kg/h of liquid hydrogen.

3 Cryogenic power electronic

Power electronics will play an indispensable role in all-electric and hybrid-electric aircraft [44], [45]. As a cryostat is needed to cool down the superconducting machine, it is better from an engineering point of view to have the entire system, including the networks to be laid out at that temperature. Thus, figure 5 shows the architecture of all-electric aircraft based on the literature [45], [46]. In the figure, the entire system, generators, power electronics, cables, and motors are located at the same temperature.

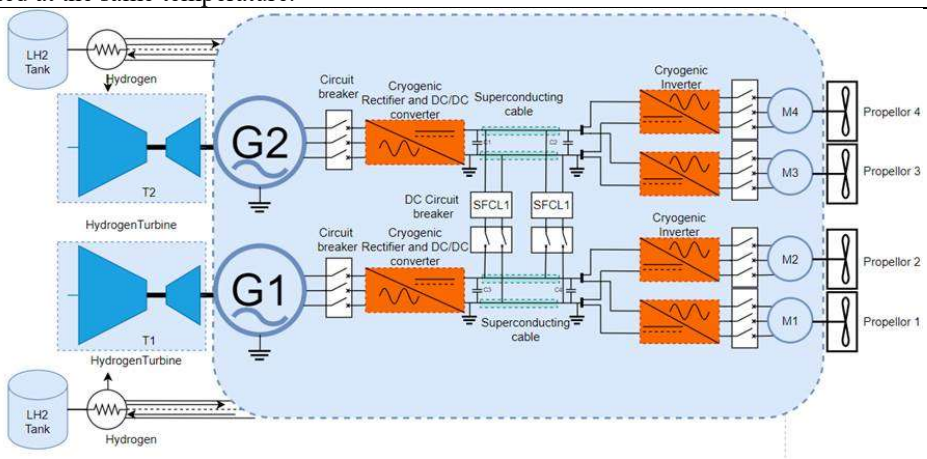

Figure 5: Architecture of all-electric aircraft

3.1 Design specifications

For this paper, the design specifications were set as seen in Table 3. Based on those requirements, the paper investigates the most suitable semiconductor devices and inverter topology. The comparison is done based on losses, reliability and complexity.

Table 3 Summary of the previously tested semiconductor devices at cryogenic temperature.

Parameter	Value
Power Rating, MW	2.3
Input voltage (DC bus), V	3000
Output voltage (AC), V	1200
Output current, A	1200

This project has received funding from the European Union's Horizon 2020 research and innovation program under grant agreement No 875006 IMOTHEP - Copyright© 2022 by IMOTHEP. Published by the EUCASS association with permission.

DOI: 10.13009/EUCASS2022-7234

3.1.1 Selection of semiconductor switch

The performance of power electronics at cryogenic temperature has been reviewed in [47]. to identify the behaviour of different semiconductor switches at temperatures below ambient. Table 4 shows a review of semiconductor devices tested at a lower temperature. From the table, it can be seen that the Si MOSFETs, IGBTs and GaN HEMTs/HFETs are the best options for devices at cryogenic temperature as their performance improves with the decrease of temperature. GaN HEMTs/HFETs are known to exhibit a kink effect at a cryogenic temperature [48],[49]. Off-the-shelf Si MOSFETs are only available at a rating below 600 V and 200 A, thus to supply power at the MW level, they require configuration to connect them in parallel and series. Based on this, the best semiconductor option for a converter at the power level of MW would be IGBTs.

Table 4 Summary of the previously tested semiconductor devices at cryogenic temperature.

		Devices					
		Diode	SiC MOSFET	Si MOSFET	IGBT	GaN HEMT	JFET
Characteristic	Forward Voltage	Increases by 20-260% for all devices but GaAS which decreases by 20%	-	-	Decreases by 5-30%	-	-
	Gate-source threshold voltage	-	Increases by 50%	Increases by 50%	Increases by 20%	Range from: -35% to +15%	Not mentioned in the reviewed literature
	On-state resistance	Decrease for (20-70%): Silicon diode MBRS Schottky ES2A Superfast Increased for (20-80%) Silicon Ultrafast Silicon Schottky Cree SiC	Increases by 300%	Decreases by 80-95%	Decreases by 30-70%	Decreases by 80-90%	Decreases (the exact amounts not mentioned in the reviewed literature)
	Breakdown Voltage	Increased by 5% SiC Schottky Cree SiC ES2A Superfast Decreased by 20% MBRS Schottky Ultrafast Diode Silicon Schottky	Decreases by 20%	Decreases by 15-35%	Decreases by 20-70%	0%	Sparse data
	Switching Time	Reverse recovery time decreases by 30%	Sparse data	Rise and fall time decrease by 60%	Decrease by 60-80%	Lower switching losses (Not specified in literature)	Sparse data

3.1.2 Selection of inverter topology

The technological advancement of the semiconductor devices and the diverse application of inverters for machine drives the requirements to achieve high efficiency and low total harmonic distortion (THD) has driven the necessity

This project has received funding from the European Union's Horizon 2020 research and innovation program under grant agreement No 875006 IMOTHEP - Copyright© 2022 by IMOTHEP. Published by the EUCASS association with permission.

DOI: 10.13009/EUCASS2022-7234

for new and innovative inverter topologies. In this section, a quick review of inverter topologies and the best topology that would be suited for cryogenic temperature are presented.
In [50] different types of indirect inverters were investigated, which can be classified into two main categories: 1) current source inverters, that operate at constant current as input, and 2) voltage source inverters, that operate at constant voltage as input. For large power applications, current source inverters and load-commutated inverters (LCI) are used as they're reliable, have lower cost, and are simple to use and implement. However, they suffer from issues such as the low-input power factor and distorted current waveforms. However, the dominant converters in the market currently are the voltage source inverters, simply because when an IGBT switch is employed, the conduction losses of the current source inverter are almost double that of the voltage source inverter, as they require a series diode to provide reverse-voltage-blocking capability [51]. As for the voltage source inverters, were developed to reach the higher operating voltage. The extra switches and sources are usually used to produce different output-voltage levels, thus producing a stepped waveform that would offer lower harmonic distortion than usual topologies, and reduce dv/dt's and common-mode voltages, as well as through operation under fault conditions and converter modularity. For the multilevel inverter the three most common topologies are as follows a) neutral point clamped (NPC/ANPC), b) flying capacitor and c) capacitor H-Bridge (CHB).
As seen in
Table [52], a comparison was done between 2 level voltage source inverter (2L-VSI) and neutral point clamped, where it had been concluded that this should not be applied in applications where a high converter efficiency and a low THD (below 5%) for the output voltage are required. Furthermore, the 2L-VSI is not attractive for high switching frequency medium voltage applications since the high switching losses caused by the maximum commutation voltage strongly limit the switch utilization and the maximum switching frequency. Also in [54], a comparison was presented among 3-level neutral (3L-NPC) point clamped, 3-level and 4-level flying capacitor inverters (3L-FLC, 4L-FLC). The 4L-FLC was shown as a non-attractive option, mainly as it has a larger number of components in series making it less reliable. The 3L-FLC was very attractive if a limited output filter is required, as they can operate at a higher switching frequency and they also have the advantage of utilising fewer power components than the 3L-NPC. However, 3L-NPC has the highest efficiency and they don't require high switching frequency operation. In [53] a comparison among 3L-NPC, 3L-FLC and 9L-CHB was done, where the 3L-NPC inverter has shown the highest efficiency. Nevertheless, the 9L-CHB is attractive for medium voltage applications due to its fault ride-through capability.

Table 5 comparison between different multilevel converters

Type of converter	Advantages	Disadvantages
2L-VSI	-Simple control -Small number of switches	-Switches need to have a large breakdown voltage -Large THD -Efficiency lower than other converters
3L-NPC	-Highest efficiency -Low THD	-Complicated control -Unequal loss distribution
3L-ANPC	-Highest efficiency -Low THD	-Complicated control
4L-NPC	-High efficiency	-A large number of series components, lower efficiency
3L-FLC	-Small filter is required at the output -High efficiency	-Complicated control
9L-CHB	-Good fault ride-through capability -Modular -High efficiency	-Complicated control

Both the 3L-NPC and 3L-ANPC are the best candidates for cryogenic temperature inverters mainly due to their high efficiency and good reliability. NPC has some structural drawbacks, [54] such as the unequal loss distribution resulting in unsymmetrical temperature distribution. If active switches are used instead of the diodes, then the unequal loss issue can be significantly improved. Figure 6 shows the ANPC inverter schematic proposed for driving the HTS motor.

This project has received funding from the European Union's Horizon 2020 research and innovation program under grant agreement No 875006 IMOTHEP

DOI: 10.13009/EUCASS2022-7234

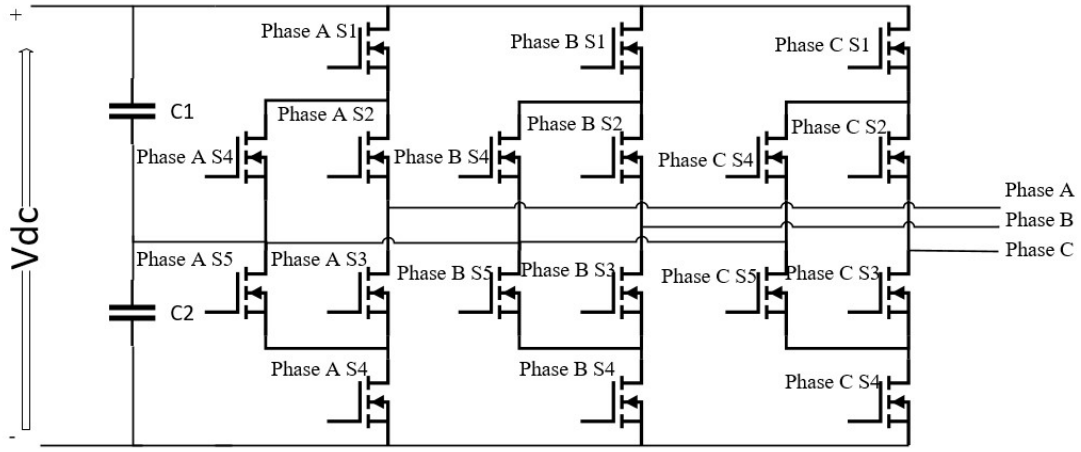

Figure 6: ANPC inverter

3.1.3 Inverter efficiency and weight estimation

In [55], it has built a simulation for NPT IGBT DIM200MHS17-A000 was used in a 2L-VSI, where the simulation has shown that there was an improved efficiency of the inverter from 86.6% at room temperature to 95.3% at 50K. Thus, an increase in of efficiency about 2-10% for inverters was observed when working at cryogenic temperature rather than room temperature.

The weight of the inverter comes mainly from the IGBTs, capacitors, and wire or busbar connections. Two different IGBT packages were selected to build the inverter 1) FF1800R17IP5BPSA1, in standard module packaging with a voltage rating of 1700 V and current rating of 1800 A and 2) 5SNA 1600N170100 with press pack packaging with a voltage rating of 4500 V and rating of current 2000 A. The weight of the switches is the easiest to determine as they are available in the manufacturer's datasheet and can be seen in Table 5. However, the values of capacitors require more simulation to estimate the filter requirement. The connection weight can be obtained through calculations. From Table 5, it can be seen that the standard packaging would weigh less at cryogenic temperature, however, thermal cycling tests need to be performed on both devices to understand which is more robust and can withstand such extreme conditions.

Table 1 weight of different converter components

Type	Device	Manufacturer	Weight (grams)	Total weight of the inverter (grams)
IGBT(9 modules)	FF1800R17IP5BPSA1	Infineon	1400/unit	12,600
	5SNA 2000K450300 (Press pack)	ABB	4300/unit	38,700
Capacitors	Polypropylene	-	300-400/unit	300-400
Connections	Copper bar	-	650/module+ interconnections	5,000 (initial estimate)
Total (option 1)	Standard packaging (initial estimate)			18,000
Total (option 2)	Press pack (initial estimate)			44,100

4. Conclusion

The use of power electronics at cryogenic temperature was investigated. Where, based on the literature, it was found that the most suitable devices to build inverter circuits would be IGBTs as the high voltage and current rating thus eliminating the need of using complicated circuitry. A quick review was also made on the most suitable inverter topology, where it was deduced that a 3L-ANPC would be able to have low harmonics output and the highest efficiency. In the end, a calculation was done to determine the weight of the inverter, where according to the initial calculations a standard pack would be lighter and more practical, however, further experimental studies are needed to confirm that these are the most suitable devices for that application.

This project has received funding from the European Union's Horizon 2020 research and innovation program under grant agreement No 875006 IMOTHEP - Copyright© 2022 by IMOTHEP. Published by the EUCASS association with permission.

It is possible with a fully superconducting machine to achieve a very high-power density. Torque oscillations are low, less than 10% for all configurations. The main remaining problem is that of optimization, considering the losses in the superconductors and the non-active elements of the machine.
The power obtained for the superconducting motor is higher than that required, and the adjustments needed to place the non-active elements will most certainly decrease this power (not only the specific power). Furthermore, as the operating times of the motor are not defined This implies that the power ratings of the motors are oversized. The given power ratings, therefore, correspond to steady state operation. In an optimized design, a distinction is made between transient operation, even for a few minutes, and steady state operation.

References

[1] J. Olivier and J. Peters, "Trends in Global CO2 and Total Greenhouse Gas Emissions; 2020 Report," PBL Netherlands Environmental Assessment Agency, Dec. 2020. [Online]. Available: https://www.pbl.nl/en/publications/trends-in-global-co2-and-total-greenhouse-gas-emissions-2020-report
[2] "Global Energy Review 2021," IEA, Paris. [Online]. Available: https://www.iea.org/reports/global-energy-review-2021
[3] Joint Research Centre (European Commission) et al., Fossil CO2 and GHG emissions of all world countries: 2019 report. LU: Publications Office of the European Union, 2019. Accessed: Mar. 02, 2022. [Online]. Available: https://data.europa.eu/doi/10.2760/687800
[4] "CO2 emissions from commercial aviation: 2013, 2018, and 2019," International Council on Clean Transportation. https://theicct.org/publication/co2-emissions-from-commercial-aviation-2013-2018-and-2019/ (accessed Feb. 18, 2022).
[5] J. A. Rosero, J. A. Ortega, E. Aldabas, and L. Romeral, "Moving towards a more electric aircraft," IEEE Aerospace and Electronic Systems Magazine, vol. 22, no. 3, pp. 3–9, Mar. 2007, doi: 10.1109/MAES.2007.340500.
[6] M. Sinnett, "787 No-Bleed Systems: Saving Fuel and enhancing operational efficiencies," Aero Quarterly, vol. 18, pp. 6–11, 2007.
[7] B. Sarlioglu and C. T. Morris, "More Electric Aircraft: Review, Challenges, and Opportunities for Commercial Transport Aircraft," IEEE Transactions on Transportation Electrification, vol. 1, no. 1, pp. 54–64, Jun. 2015, doi: 10.1109/TTE.2015.2426499.
[8] J. L. Felder, "NASA Electric Propulsion System Studies," Nov. 30, 2015. Accessed: Sep. 23, 2019. [Online]. Available: https://ntrs.nasa.gov/search.jsp?R=20160009274
[9] R. H. Jansen, C. L. Bowman, A. Jankovsky, R. Dyson, and J. L. Felder, "Overview of NASA electrified aircraft propulsion research for large subsonic transports."
[12] G. Girishkumar, B. McCloskey, A. C. Luntz, S. Swanson, and W. Wilcke, "Lithium−Air Battery: Promise and Challenges," J. Phys. Chem. Lett., vol. 1, no. 14, pp. 2193–2203, Jul. 2010, doi: 10.1021/jz1005384.
[10] T. Bærheim, J. J. Lamb, J. K. Nøland, and O. S. Burheim, "Potential and Limitations of Battery-Powered All-Electric Regional Flights -- A Norwegian Case Study," Mar. 2022, doi: 10.36227/techrxiv.19382585.v1.
[11] M. Voskuijl, J. van Bogaert, and A. G. Rao, "Analysis and design of hybrid electric regional turboprop aircraft," CEAS Aeronaut J, vol. 9, no. 1, pp. 15–25, Mar. 2018, doi: 10.1007/s13272-017-0272-1.
[13] R. Jansen, G. V. Brown, J. L. Felder, and K. P. Duffy, "Turboelectric Aircraft Drive Key Performance Parameters and Functional Requirements," in 51st AIAA/SAE/ASEE Joint Propulsion Conference, American Institute of Aeronautics and Astronautics. doi: 10.2514/6.2015-3890.
[14] "Electric propulsion components with high power densities for aviation," presented at the Transformative Vertical Flight Workshop, Mar. 08, 2015.
[15] A. El-Refaie and M. Osama, "High specific power electrical machines: A system perspective," CES Transactions on Electrical Machines and Systems, vol. 3, no. 1, pp. 88–93, Mar. 2019, doi: 10.30941/CESTEMS.2019.00012.

This project has received funding from the European Union's Horizon 2020 research and innovation program under grant agreement No 875006 IMOTHEP

[16] P. Lindh, I. Petrov, J. Pyrhönen, E. Scherman, M. Niemelä, and P. Immonen, "Direct Liquid Cooling Method Verified With a Permanent-Magnet Traction Motor in a Bus," IEEE Transactions on Industry Applications, vol. 55, no. 4, pp. 4183–4191, Jul. 2019, doi: 10.1109/TIA.2019.2908801.
[17] S. Ayat, "An Experiment-Informed Methodology for the Thermal Design of Permanent Magnet Electrical Machines," University of Bristol, 2018.
[18] D. Golovanov et al., "4MW Class High Power Density Generator for Future Hybrid-Electric Aircraft," IEEE Transactions on Transportation Electrification, pp. 1–1, 2021, doi: 10.1109/TTE.2021.3068928.
[19] G. Brown, "Weights and Efficiencies of Electric Components of a Turboelectric Aircraft Propulsion System," in 49th AIAA Aerospace Sciences Meeting including the New Horizons Forum and Aerospace Exposition, 0 vols., American Institute of Aeronautics and Astronautics, 2011. doi: 10.2514/6.2011-225.
[21] C. D. Manolopoulos, M. F. Iacchetti, A. C. Smith, K. Berger, M. Husband, and P. Miller, "Stator Design and Performance of Superconducting Motors for Aerospace Electric Propulsion Systems," IEEE Trans. Appl. Supercond., vol. 28, no. 4, pp. 1–5, Jun. 2018, doi: 10.1109/TASC.2018.2814742.
[22] M. Corduan, M. Boll, R. Bause, M. P. Oomen, M. Filipenko, and M. Noe, "Topology Comparison of Superconducting AC Machines for Hybrid Electric Aircraft," IEEE Transactions on Applied Superconductivity, vol. 30, no. 2, pp. 1–10, Mar. 2020, doi: 10.1109/TASC.2019.2963396.
[23] T. Winkler, "The EcoSwing Project," IOP Conf. Ser.: Mater. Sci. Eng., vol. 502, p. 012004, Apr. 2019, doi: 10.1088/1757-899X/502/1/012004.
[24] Y. Wang, J. Sun, Z. Zou, Z. Wang, and K. T. Chau, "Design and Analysis of a HTS Flux-Switching Machine for Wind Energy Conversion," IEEE Transactions on Applied Superconductivity, vol. 23, no. 3, pp. 5000904–5000904, Jun. 2013, doi: 10.1109/TASC.2013.2242113.
[25] D. Torrey et al., "Superconducting Synchronous Motors for Electric Ship Propulsion," IEEE Transactions on Applied Superconductivity, vol. 30, no. 4, pp. 1–8, Jun. 2020, doi: 10.1109/TASC.2020.2980844.
[26] G. Snitchler, B. Gamble, and S. S. Kalsi, "The performance of a 5 MW high temperature superconductor ship propulsion motor," IEEE Transactions on Applied Superconductivity, vol. 15, no. 2, pp. 2206–2209, Jun. 2005, doi: 10.1109/TASC.2005.849613.
[27] M. Filipenko et al., "Concept design of a high power superconducting generator for future hybrid-electric aircraft," Supercond. Sci. Technol., vol. 33, no. 5, p. 054002, Mar. 2020, doi: 10.1088/1361-6668/ab695a.
[28] H. J. M. ter Brake and G. F. M. Wiegerinck, "Low-power cryocooler survey," Cryogenics, vol. 42, no. 11, pp. 705–718, Nov. 2002, doi: 10.1016/S0011-2275(02)00143-1.
[29] K. S. Haran et al., "High power density superconducting rotating machines—development status and technology roadmap," Supercond. Sci. Technol., vol. 30, no. 12, p. 123002, Nov. 2017, doi: 10.1088/1361-6668/aa833e.
[30] R. Radebaugh, "Cryocoolers for aircraft superconducting generators and motors," AIP Conference Proceedings, vol. 1434, no. 1, pp. 171–182, Jun. 2012, doi: 10.1063/1.4706918.
[31] J. Palmer and E. Shehab, "Modelling of cryogenic cooling system design concepts for superconducting aircraft propulsion," IET Electrical Systems in Transportation, vol. 6, no. 3, pp. 170–178, 2016, doi: 10.1049/iet-est.2015.0020.
[32] M. Noe, "Superconducting Cable," Sep. 17, 2017. [Online]. Available: https://indico.cern.ch/event/626654/attachments/1523851/2381785/Superconducting_Cables_-_Dr._Mathias_Noe.pdf
[33] S. Schlachter, W. Golddacker, B. Holzapfel, A. Kudymow, and H. Wu, "Design Aspects for DC HTS Cables in Hybrid Electric Propulsion Systems for Aircraft," presented at the CEC-ICMC, Madison, Wisconsin, USA, Jul. 11, 2017.
[34] A. Elwakeel, Z. Feng, N. McNeill, M. Zhang, B. Williams, and W. Yuan, "Study of Power Devices for Use in Phase-Leg at Cryogenic Temperature," IEEE Transactions on Applied Superconductivity, vol. 31, no. 5, pp. 1–5, Aug. 2021, doi: 10.1109/TASC.2021.3064544.
[35] L. Graber et al., "Cryogenic power electronics at megawatt-scale using a new type of press-pack IGBT," IOP Conf. Ser.: Mater. Sci. Eng., vol. 279, p. 012011, Dec. 2017, doi: 10.1088/1757-899X/279/1/012011.

This project has received funding from the European Union's Horizon 2020 research and innovation program under grant agreement No 875006 IMOTHEP - Copyright© 2022 by IMOTHEP. Published by the EUCASS association with permission.

[36] M. Mehrabankhomartash et al., “Static and Dynamic Characterization of 650 V GaN E-HEMTs in Room and Cryogenic Environments,” in 2021 IEEE Energy Conversion Congress and Exposition (ECCE), Oct. 2021, pp. 5289–5296. doi: 10.1109/ECCE47101.2021.9595593.
[37] F. Weng, M. Zhang, A. Elwakeel, T. Lan, N. McNeill, and W. Yuan, “Transient Test and AC Loss Study of a Cryogenic Propulsion Unit for All Electric Aircraft,” IEEE Access, vol. 9, pp. 59628–59636, 2021, doi: 10.1109/ACCESS.2021.3073071.
[38] H. Gui et al., “Review of Power Electronics Components at Cryogenic Temperatures,” IEEE Transactions on Power Electronics, vol. 35, no. 5, pp. 5144–5156, May 2020, doi: 10.1109/TPEL.2019.2944781.
[39] R. Chen and F. F. Wang, “SiC and GaN Devices With Cryogenic Cooling,” IEEE Open Journal of Power Electronics, vol. 2, pp. 315–326, 2021, doi: 10.1109/OJPEL.2021.3075061.
[41] R. Chen, Z. Yang, and F. Wang, “Overcurrent and Short-circuit Capability Experimental Investigation for GaN HEMT at Cryogenic Temperature,” in 2021 IEEE Applied Power Electronics Conference and Exposition (APEC), Jun. 2021, pp. 382–388. doi: 10.1109/APEC42165.2021.9487188.
[89] F. Wang et al., “MW-Class Cryogenically-Cooled Inverter for Electric-Aircraft Applications,” in 2019 AIAA/IEEE Electric Aircraft Technologies Symposium (EATS), Aug. 2019, pp. 1–9. doi: 10.2514/6.2019-4473.
[24] S. C. Wimbush and N. M. Strickland, “A Public Database of High-Temperature Superconductor Critical Current Data,” IEEE Transactions on Applied Superconductivity, vol. 27, no. 4, pp. 1–5, Jun. 2017, doi: 10.1109/TASC.2016.2628700.
[43] S. Wimbush and N. Strickland, “A high-temperature superconducting (HTS) wire critical current database,” Oct. 2019, doi: 10.6084/m9.figshare.c.2861821.v10.
[44] A. Barzkar and M. Ghassemi, “Electric Power Systems in More and All Electric Aircraft: A Review,” in *IEEE Access*, vol. 8, pp. 169314-169332, Sept. 2020
[45] K. Nøland, "Hydrogen Electric Airplanes: A disruptive technological path to clean up the aviation sector," in *IEEE Electrification Magazine*, vol. 9, no. 1, pp. 92-102, Mar. 2021
[46] S. Venuturumilli, F. Berg, M. Zhang, and W. Yuan, “Investigation of HTS Cable Impact on turbo-electric aircraft performance*,” IET Electrical Systems in Transportation*, vol. 10, no. 1, pp. 62–67, 2020.
[47] K. Rajashekara and B. Akin, “A review of cryogenic power electronicsstatus and applications,” in *Proc. IEEE Int. Elect. Mach.* Drive, pp. 899-904 , July, 2013.
[48] R. Cuerdo *et al.*, “The kink effect at cryogenic temperatures in deep submicron AlGaN/GaN HEMTs,” *IEEE Electron Device Lett.*, vol. 30, no. 3, pp. 209–212, 2009.
[49] I. M. Hafez, G. Ghibaudo, and F. Balestra, “Analysis of the kink effect In MOS transistors,” *IEEE Trans. Electron Devices*, vol. 37, no. 3, pp. 818–821, 1990.
[50] J. Rodriguez, S. Bernet, B. Wu, J. O. Pontt and S. Kouro, "Multilevel Voltage-Source-Converter Topologies for Industrial Medium-Voltage Drives," in IEEE Transactions on Industrial Electronics, vol. 54, no. 6, pp. 2930-2945, Dec. 2007
[51] R. A. Torres, H. Dai, W. Lee, T. M. Jahns and B. Sarlioglu, "Current-Source Inverters for Integrated Motor Drives using Wide-Bandgap Power Switches," *IEEE Transp. Electrification Conf. and Expo (ITEC)*, 2018, pp. 1002-1008
[52] D. Krug, M. Malinowski and S. Bernet, "Design and comparison of medium voltage multi-level converters for industry applications," Conference Record of the 2004 IEEE Industry Applications Conference, 2004. 39th IAS Annual Meeting., 2004, pp. 781-790 vol.2
[53] S. S. Fazel, S. Bernet, D. Krug and K. Jalili, "Design and Comparison of 4-kV Neutral-Point-Clamped, Flying-Capacitor, and Series-Connected H-Bridge Multilevel Converters," in *IEEE Transactions on Industry Applications*, vol. 43, no. 4, pp. 1032-1040, July-augc. 2007
[54] J. Rodriguez, S. Bernet, P. K. Steimer and I. E. Lizama, "A Survey on Neutral-Point-Clamped Inverters," in *IEEE Transactions on Industrial Electronics*, vol. 57, no. 7, pp. 2219-2230, July 2010
[55] S. Yang, “Cryogenic characteristics of IGBTs,” PhD thesis, University of Birmingham, 2005.

This project has received funding from the European Union’s Horizon 2020 research and innovation program under grant agreement No 875006 IMOTHEP - Copyright© 2022 by IMOTHEP. Published by the EUCASS association with permission.